High Temperatures-High Pressures, Vol. 52, pp. 195–210
Reprints available directly from the publisher
Photocopying permitted by license only
DOI: 10.32908/hthp.v52.1437

$AlO_{1.5}/SiO_2$ substitution effect on the viscosity of alkali silicate melts

S. Sukenaga[1]*, R. Ikoma[1,2], M. Tashiro[1], Y. Chiba[1], S. Kawanishi[1] and H. Shibata[1]

[1]*Institute of Multidisciplinary Research for Advanced Materials (IMRAM), Tohoku University, 2-1-1 Katahira, Aoba-ku, 980-8577 Sendai, Japan*
[2]*Graduate School of Engineering, Tohoku University, 6-6, Aramaki Aza Aoba, Aoba-ku, Sendai 9808579, Japan*

Received: February 4, 2023; Accepted: February 14, 2023.

The effect of alumina addition on the viscosity of silicate melts is strongly related to the type of non-framework cations; however, the origin of these interactions is not well understood. In this study, we measured the viscosity change in selected alkali disilicate ($R_2O{\cdot}2SiO_2$, R: Na or Li) melts by varying the $AlO_{1.5}/SiO_2$ molar ratio ($AlO_{1.5}$ = 0–16.8 mol%) within the 1373–1823 K temperature range. We observed that as the molar ratio increased, sodium silicate viscosity increased, whereas lithium silicate viscosity was not affected. Aluminum-27 nuclear magnetic resonance spectra of the quenched glasses indicated that the aluminum cations in both types of alkali silicate melts were mostly present as AlO_4 tetrahedra. In contrast to sodium-containing systems, the shear strain on the AlO_4 tetrahedron was greater for lithium aluminosilicate glass. Our findings indicated that the degree of shear strain on AlO_4 plays an essential role in controlling the viscosity of aluminosilicate systems.

Keywords: Viscosity, Glass transition temperature, Alkali aluminosilicate melt, Raman spectroscopy, ^{27}Al NMR, Glass structure

*Corresponding author: sohei.sukenaga.d3@tohoku.ac.jp

1 INTRODUCTION

When a silicate melt comes into contact with molten metal containing aluminum, the silica (SiO_2) in the melt is reduced by aluminum [1, 2], as expressed by the following equation (1):

$$4\underline{Al} + 3(SiO_2) = 4(AlO_{1.5}) + 3\underline{Si} \quad (1)$$

As a result of this reaction, the molar ratio of $AlO_{1.5}$ to SiO_2 ($AlO_{1.5}/SiO_2$) in the silicate melts increases. This phenomenon occurs during the continuous casting process of aluminum-containing molten steel, which uses a silicate melt as a lubricant between the solidified steel and the mold, that is, mold flux [3]. The effect of the $AlO_{1.5}/SiO_2$ molar ratio on silicate melt viscosity is important for understanding melt fluidity and lubrication by silicate melts [4–7]. Variations in viscosity with respect to the Al_2O_3/SiO_2 molar ratio have been reported for multicomponent compositions that are similar to practical mold flux [8–13]. These studies indicate that the effect of $AlO_{1.5}/SiO_2$ on viscosity depends on the type and concentration of non-framework cations (e.g., Ca^{2+}, Mg^{2+}, Li^+, Na^+) in the silicate melt; however, the interaction between the "type of non-framework cations" and "viscosity variation with $AlO_{1.5}/SiO_2$ ratio" is not well understood. It is essential to select simple systems containing only one type of non-framework cation in order to properly understand this interaction.

When aluminum cations are present as AlO_4 tetrahedra in the silicate network structure, non-framework cations are required to compensate for the negative charge around the bridging oxygen (BO) between silicon and aluminum cations (i.e., $Si–O_{BO}–Al$) [14]. The AlO_4 tetrahedron requires a charge of $+1$ to maintain charge neutrality in the vicinity of $Si–O_{BO}–Al$. Therefore, alkali aluminosilicate ($R_2O–Al_2O_3–SiO_2$) compositions can be categorized into three types depending on the atomic ratio of the alkali and aluminum cations (R^+/Al^{3+}): peralkaline ($R^+/Al^{3+} > 1$), tectosilicate ($R^+/Al^{3+} = 1$), and peraluminous ($R^+/Al^{3+} < 1$) [15]. In peralkaline and tectosilicate compositions, aluminum cations tend to adopt four-fold coordination with oxygen atoms (AlO_4), whereas aluminum cations in five- (AlO_5) and/or six-fold coordination (AlO_6) are also present in peraluminous compositions [15]. In addition, AlO_4 species are generally more stable in alkali-silicate melts than in alkaline-earth aluminosilicate systems [14]. In the peralkaline region, the simple coordination of aluminum cations (i.e., mainly AlO_4) facilitated the investigation of the influence of the $AlO_{1.5}/SiO_2$ molar ratio on the viscosity of the alkali silicate melts. Mold fluxes usually contain calcium oxide (CaO), but an alkali oxide-containing system is more suitable for isolating the non-framework cation interactions from the AlO_4 species, significantly simplifying the fundamental studying of the viscosity. In the present study, we compared the effect of the $AlO_{1.5}/SiO_2$ molar ratio on the viscosity of sodium disilicate ($Na_2O{\cdot}2SiO_2$) and lithium disilicate ($Li_2O{\cdot}2SiO_2$) systems in the peralkaline region (molar content of $AlO_{1.5} = 0$–16.8 mol%) and the temperature range of 1372–1823 K.

2 EXPERIMENTAL

2.1 Sample synthesis

The nominal compositions of the samples are listed in Table 1. The parent compositions of the samples are similar to those of lithium disilicate ($Li_2O{\cdot}2SiO_2$) and sodium disilicate ($Na_2O{\cdot}2SiO_2$). SiO_2 in these alkali silicates was partially replaced by $AlO_{1.5}$. The samples were labeled as LAS*x* for the lithium-containing system and NAS*x* for the sodium-containing system, where *x* represented the molar content of $AlO_{1.5}$ (mol%). The parent alkali silicate contained 33 mol% Li_2O or Na_2O. The reagent powders of Na_2CO_3 (Sigma-Aldrich Co. LLC), Li_2CO_3 (Sigma-Aldrich Co. LLC), Al_2O_3 (Sigma-Aldrich Co. LLC), and SiO_2 (FUJIFILM Wako Pure Chemical Corporation) were carefully weighed and mixed using a mullite mortar and pestle. The powder mixtures were melted in a 30 ml platinum crucible in air at temperatures above their liquidus. The molten samples were then quenched using a Cu plate. The glassy samples obtained were used for viscosity measurements.

TABLE 1
Nominal compositions of the samples. The analyzed compositions after viscosity measurements are shown in parentheses.

Sample	Composition (mol%)				$AlO_{1.5}/SiO_2$ ratio	T_g/K
	Li_2O	Na_2O	$AlO_{1.5}$	SiO_2		
NAS0	–	33 (33.0)	–	67.0 (67.0)	0	721
NAS11.2	–	33 (32.7)	11.2 (11.7)	55.8 (55.7)	0.20 (0.21)	750
NAS16.8	–	33 (33.2)	16.8 (17.1)	50.2 (49.7)	0.33 (0.34)	780
LAS0	33 (32.4)	–	–	67.0 (67.6)	0	731
LAS11.2	33 (33.3)	–	11.2 (11.4)	55.8 (55.3)	0.20 (0.21)	738
LAS16.8	33 (32.5)	–	16.8 (17.0)	50.2 (50.5)	0.33 (0.34)	742

2.2 Viscosity measurements

The selection of the measurement techniques for melt viscosity depends on the viscosity range of the sample [16]. Herein, the rotating crucible method was employed to evaluate the viscosity of the samples in the range of 0.1–30 Pa·s. Detailed information regarding the viscometer has been provided in previous works [17–19]. The samples (∼40 g) were placed in a Pt–20mass%Rh crucible (inner diameter: 30 mm, height: 27 mm) and heated to 1833 K in air. Then, a bob (diameter: 15 mm, height: 8 mm) made of a Pt–20mass%Rh alloy was immersed in the melt to an immersion depth of 10 mm. The samples were melted for 60 min at 1833 K to ensure compositional homogeneity. After melting, the viscosity was measured at a crucible rotation speed of 60 rpm during the cooling process in the temperature range of 1823–1373 K at 50 K increments. At each temperature, the samples were

melted for more than 30 min to ensure the temperature homogeneity of the melt. It is well known that alkali species evaporate easily from melts. Therefore, the compositions of the quenched samples after the viscosity measurements were also analyzed. The concentrations of SiO_2 and $AlO_{1.5}$ were determined using inductively coupled plasma atomic emission spectrometry, and the concentrations of the alkali oxides were evaluated using atomic absorption spectrometry. The difference between the nominal and analyzed compositions was negligible (See Table 1). In addition, the crystallinity of the quenched samples was evaluated from the X-ray diffraction (XRD) patterns obtained using Cu Kα radiation. Glass transition temperature measurements and structural characterizations were performed on non-crystalline samples.

2.3 Measurement of glass transition temperature

The glass transition temperature (T_g) is a structure-sensitive characteristic temperature where the viscosity is close to 10^{12} Pa·s. Herein, the glass transition temperatures of quenched glasses after viscosity measurements were determined via differential thermal analysis (DTA) using a Thermo Plus Evo TG8120 instrument (Rigaku Corporation). The powdered samples (15 mg) were placed in a platinum cell and heated at 20 K/min in air. The obtained DTA curves were analyzed to determine T_g values.

2.4 Structural characterization

The local structures around the aluminum and silicon cations are important parameters for understanding the viscosity of aluminosilicate melts. This study characterizes this type of structural information for quenched glasses using aluminum-27 magic angle spinning nuclear magnetic resonance (^{27}Al MAS NMR) and Raman spectroscopy. ^{27}Al MAS NMR spectra were collected for the glass samples in powder form. The measurements were conducted using a Bruker Avance III 600 spectrometer (magnetic field: 14 T) equipped with a Bruker 4 mm MAS probe. The samples were packed in a 4 mm ZrO_2 container and spun at 11 kHz. Because ^{27}Al is a quadrupolar nucleus, a small tip angle (18° pulse*)* was used to obtain quantitative spectra in the single-pulse experiments [20]. The number of scans was set to 1024 with a relaxation delay of 3.5 s, which was sufficient to achieve full relaxation. The ^{27}Al chemical shifts were referenced against 1M $Al(NO_3)_3$ solution. Raman spectra were recorded using an XploRA confocal Raman microscope (Horiba Jobin Yvon). The samples were excited using a 532 nm Nd:YAG laser with an acquisition time of 50 s, and four scans were recorded for each measurement. The intensity of the obtained spectra was normalized by the integrated intensity of the spectrum (i.e., peak area) in the range of 25–2000 cm^{-1} [21].

3 RESULTS AND DISCUSSION

3.1 Viscosity

Figures 1 (a) and (b) compare the viscosities measured for the binary sodium and lithium silicate compositions in this study with reported values [17, 22–28]. As shown in Figure 1 (a), the reported data for compositions similar to NAS0 have an approximately ±40% scatter. Our data for the viscosities of

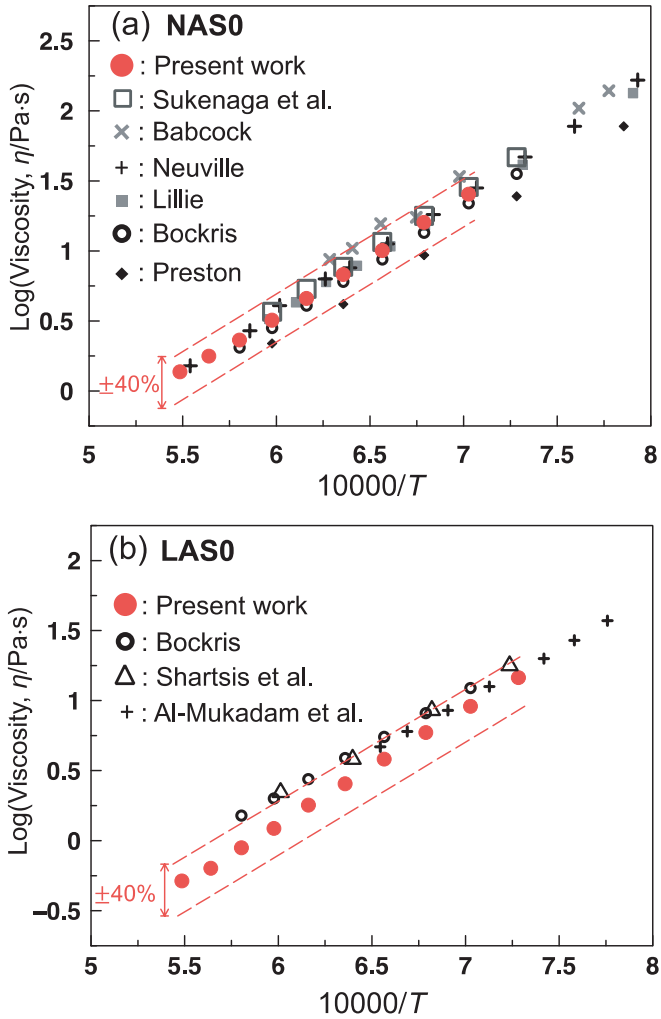

FIGURE 1
Viscosity of (a) NAS0 and (b) LAS0 melts, compared with the reported viscosities of sodium disilicate and lithium disilicate compositions. Dashed lines indicate the scatter range of ±40% from the viscosity measured in the present study.

the NAS0 and LAS0 melts were within the scatter range. The viscosities measured in this study are listed in Table 2. Figure 2 shows the temperature dependence of the logarithmic viscosity of alkali aluminosilicate melts. The logarithmic viscosity of these ternary aluminosilicate melts increased linearly with reciprocal temperature. The temperature dependence fitted well with a linear function. The slope of the NAS0 melt increased with an increase in the $AlO_{1.5}/SiO_2$ molar ratio, whereas the slopes of the lithium aluminosilicate melts (i.e., LAS11.2 and LAS16.8) were smaller than those of the binary lithium silicate melts (i.e., LAS0). Figure 3 shows the evolution of viscosity with respect to the molar content of $AlO_{1.5}$ at 1623 K. The viscosity of the sodium silicate system increased upon replacing SiO_2 with $AlO_{1.5}$, whereas the viscosity of lithium silicate melts was insensitive to the $AlO_{1.5}$ content.

TABLE 2
Viscosities of the samples measured at different temperatures.

	Viscosity, η/Pa·s					
***T* / K**	**NAS0**	**NAS11.2**	**NAS16.8**	**LAS0**	**LAS11.2**	**LAS16.8**
1823	1.38	1.44	1.56	0.516	0.639	0.544
1773	1.78	1.96	2.15	0.636	0.771	0.711
1723	2.32	2.73	3.10	0.891	0.963	0.936
1673	3.20	4.07	4.67	1.22	1.25	1.20
1623	4.58	6.40	7.31	1.80	1.65	1.72
1573	6.80	10.4	11.6	2.55	2.25	2.47
1523	10.1	16.4	20.1	3.83	3.15	3.35
1473	16.0	26.5	37.6	5.93	4.67	5.04
1423	25.5	–	–	9.11	7.36	7.71
1373		–	–	14.6	12.5	12.2

3.2 Glass transition temperature

Figure 4 shows the XRD patterns of the quenched samples after the viscosity measurements. The XRD patterns of all samples were broad, indicating that the samples were non-crystalline. These glassy samples were also used for DTA. Figures 5 (a) and (b) show the DTA curves of the alkali aluminosilicate glasses. The T_g of the samples was determined using the conventional onset method [29], which defines T_g as the intersection of the two lines tangential to the curve before and after the initiation of the glass transition (Figure 5). The observed T_g values of the NAS0 (721 K) and LAS0 (731 K) glass samples were close to the reported values (NAS0: 726 K [23] and LAS0: 733 K [30]), which validates our methodology. The exothermic

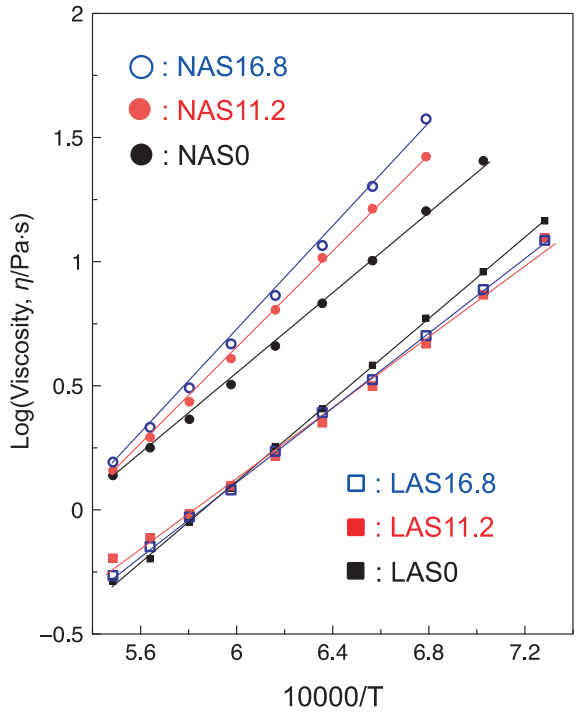

FIGURE 2
Temperature dependencies of viscosity for the sodium or lithium aluminosilicate melts.

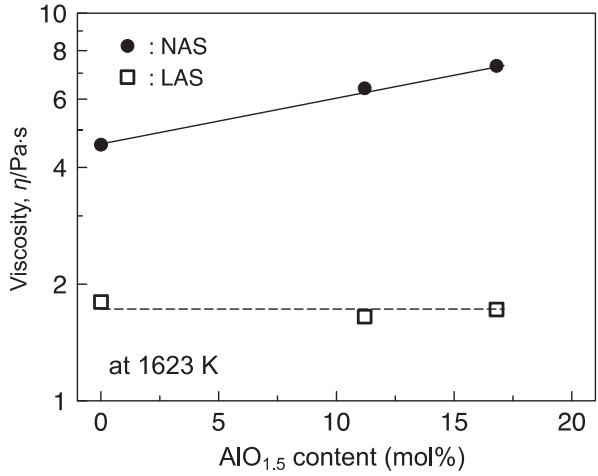

FIGURE 3
Effect of the molar content of $AlO_{1.5}$ on the viscosity of sodium or lithium aluminosilicate melts at 1623 K.

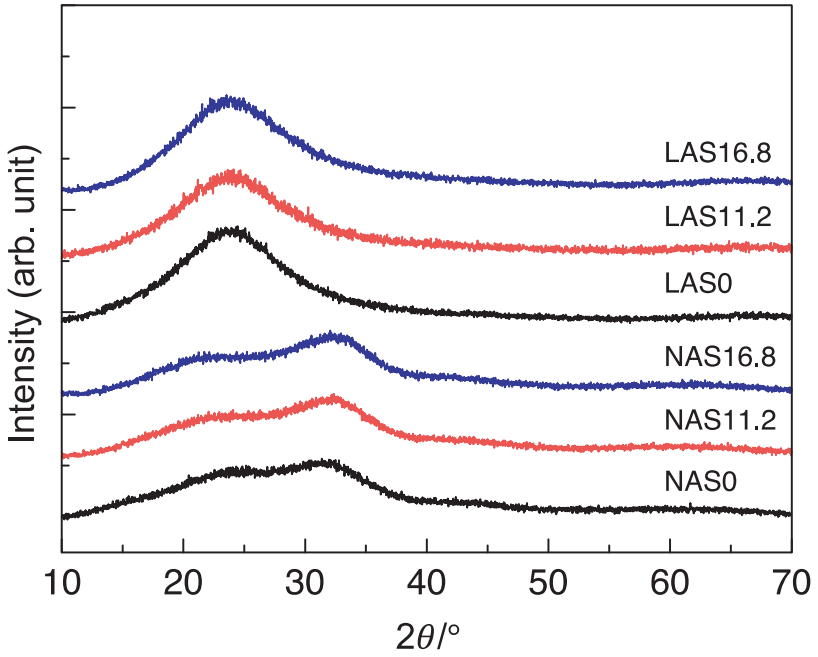

FIGURE 4
X-ray diffraction (XRD) pattern of the quenched samples after viscosity measurements.

peak at temperatures higher than T_g indicates the crystallization of the samples. Figure 6 shows the effect of $AlO_{1.5}$ content on the T_g of the samples. The T_g of the sodium silicate glass increased upon the substitution of SiO_2 with $AlO_{1.5}$, whereas the T_g was insensitive to the $AlO_{1.5}$ content in the lithium silicate glasses. The glass transition temperature exhibited a similar compositional dependence on the viscosity of the melts at temperatures above the liquidus.

3.3 Raman Spectra

Figure 7 shows the change in the Raman spectra of the alkali silicate glasses upon the substitution of SiO_2 with $AlO_{1.5}$. The Raman signals of these glasses were observed in four regions: boson (20–250 cm^{-1}), low-frequency (250–700 cm^{-1}), intermediate (750–850 cm^{-1}), and high-frequency (850–1300 cm^{-1}) [31]. Raman spectra exhibited significant variations in the low-, intermediate-, and high-frequency regions. Because little is known about the origin of the Raman signals in the intermediate-frequency region [31], in this study, we focused on the low- and high-frequency regions. Signals in the low-frequency region were assigned to the vibrations of bridging oxygen atoms associated

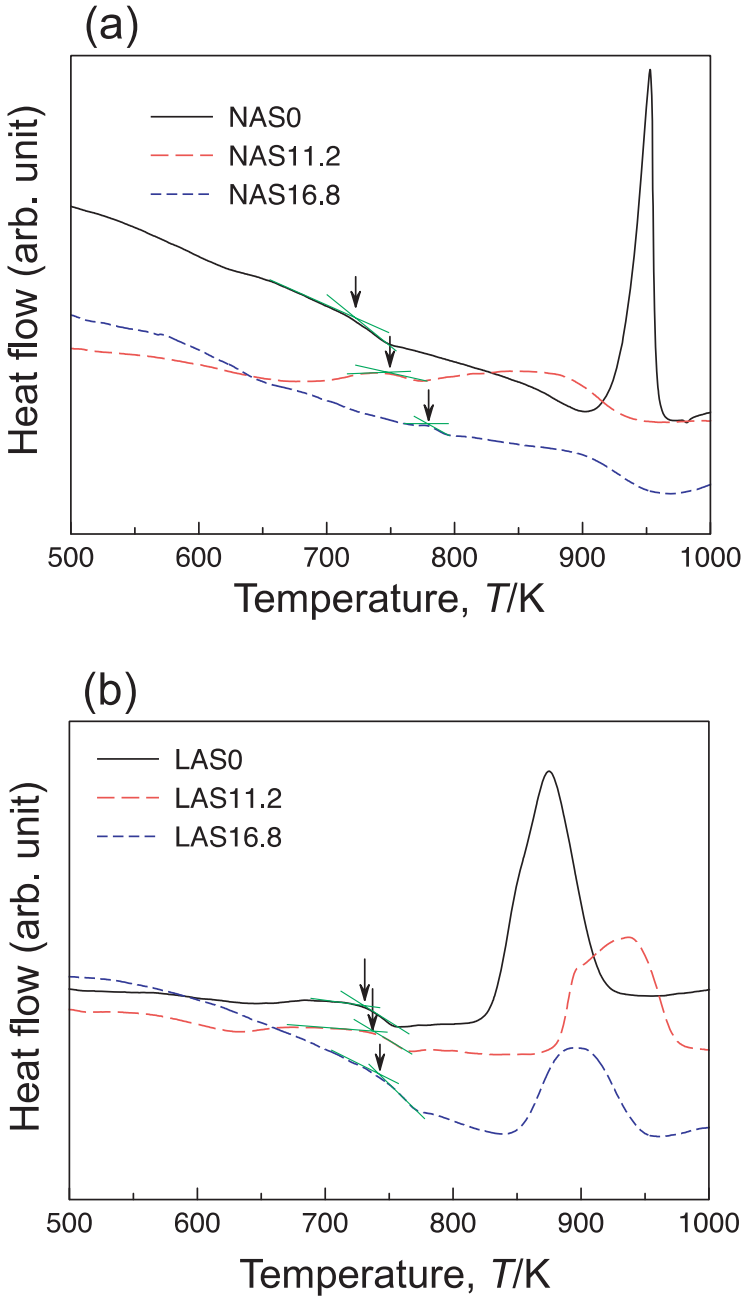

FIGURE 5
DTA curves for the quenched (a) NAS and (b) LAS glassy samples after viscosity measurements. Arrows indicate the glass transition temperatures.

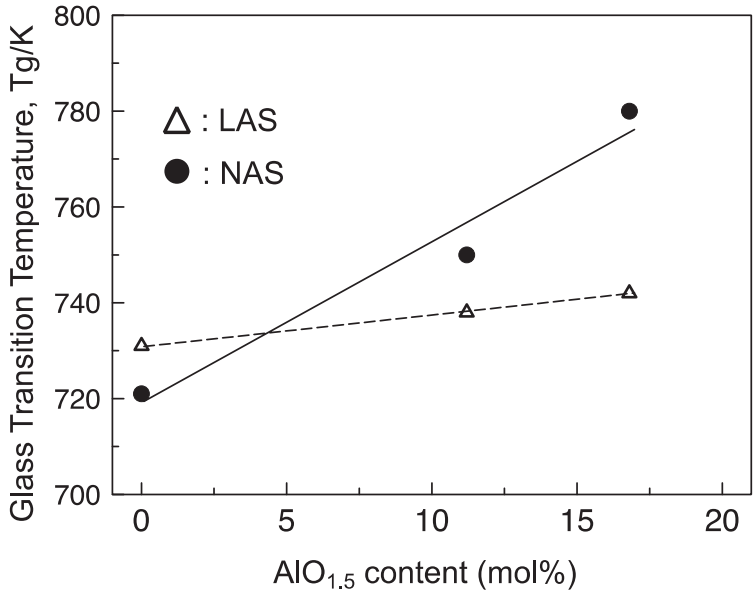

FIGURE 6
Effect of the molar content of $AlO_{1.5}$ on the T_g of the glasses.

with three-, four-, five-, or higher-membered rings of the TO_4 tetrahedra (T: Si or Al) present in the silicate network structure [32]. The NAS0 glass had a signal at approximately 570 cm^{-1}, known as the D_2 band [33], which indicated the presence of a three-membered ring. This signal broadened with increasing the molar content of $AlO_{1.5}$, indicating a variation in the T–O–T bond angle, which mainly forms a three-membered ring. A similar tendency was observed for Raman signals in the low-frequency region of the lithium aluminosilicate system. The band in the high-frequency region was assigned to the Si–O stretching vibration [34]. The peak position of this signal varies depending on the number of bridging and nonbridging oxygen atoms connected to the silicon atoms. Typically, silicon atoms in silicate glasses are categorized as Q^n (n: 0–4), where n represents the number of bridging oxygen atoms around the silicon atom. The major signal of NAS0 and LAS0 was located at approximately 1100 cm^{-1}, and was assigned to Q^3 species [35]. The peak at approximately 950 cm^{-1} indicated the presence of Q^2 species in the binary alkali silicate glasses [35]. The peak position of the Q^3 signals shifted to the low-frequency side with increasing molar content of $AlO_{1.5}$, whereas the position of the Q^2 signals did not change with respect to $AlO_{1.5}$ content for both sodium- and lithium-containing systems. Because the force constant of the Si–O bond is affected by the presence of neighboring aluminum atoms, the peak shift of the Q^3 signal indicates that the aluminum atom exists in the vicinity of the Q^3

silicon species, which have fewer alkali cations than the Q^2 species. This configuration was consistent with the results of an oxygen-17 nuclear magnetic resonance study of aluminosilicate glasses, where aluminum was mainly bonded to bridging oxygens [36, 37]. Overall, the Raman spectra of the glasses indicated that aluminum cations play the structural role of network formers in both sodium- and lithium-containing systems.

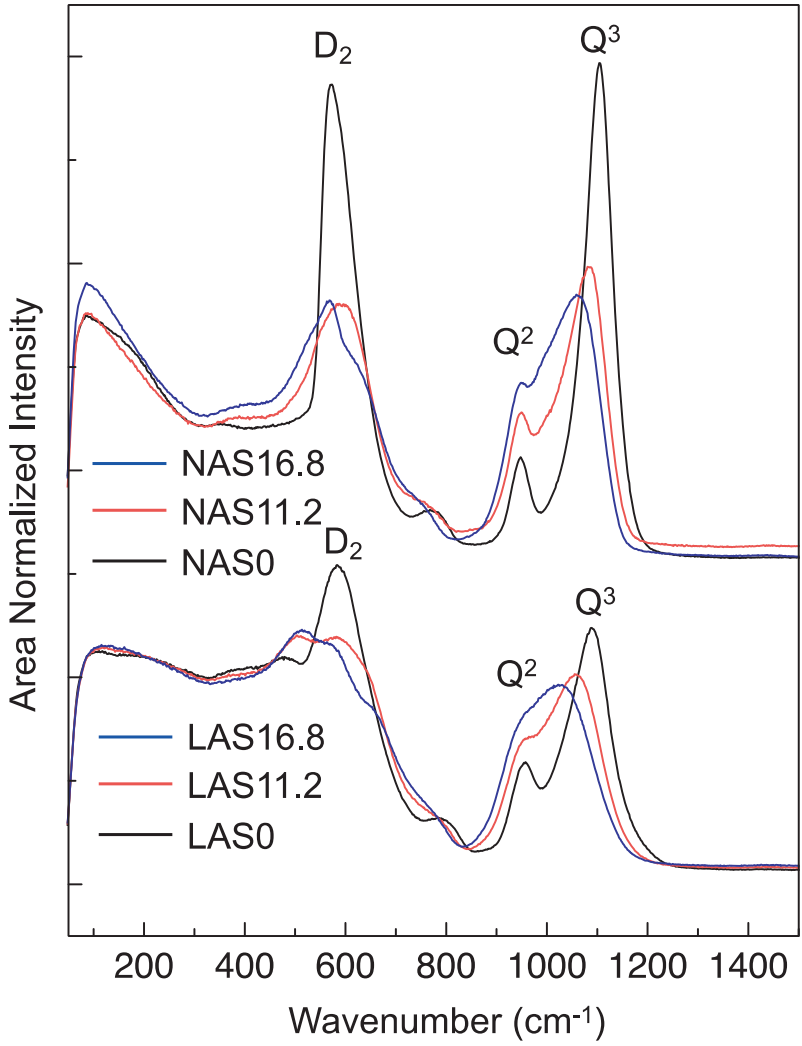

FIGURE 7
Raman spectra of the quenched glassy samples after viscosity measurements.

3.4 ^{27}Al MAS NMR

The local structure around the aluminum atoms was investigated using ^{27}Al MAS NMR spectroscopy to explain the differences between the NAS and LAS viscosities caused by $AlO_{1.5}/SiO_2$ ratios. The ^{27}Al MAS NMR spectra of alkali aluminosilicate glasses are shown in Figure 8 (a). The signals of all glasses were mainly located at approximately 65 ppm and were assigned to tetrahedrally coordinated aluminum atoms (AlO_4) [15]. The small shoulder at approximately 30 ppm for the LAS11.2 and LAS16.8 glasses indicated that a small fraction of the aluminum atoms were coordinated to five oxygen atoms (AlO_5) [15]. In addition, the line widths of the LAS glasses were greater than those of the NAS glasses. Because ^{27}Al is a quadrupolar nucleus, the signals had an asymmetric line shape, mainly due to the quadrupolar interactions, which could be characterized using a quadrupole coupling constant (C_Q) [38]. The DMFIT program [39] was used to simulate the asymmetric line shapes of the signals (see Figures 8 (b) and (c)). The fitting parameters are listed in Table 3. The content of AlO_5 species was less than 2%, and aluminum cations were mostly present as AlO_4 tetrahedra in all the glasses. Moreover, the LAS glasses had a larger C_Q than the NAS glasses. It has been reported that the C_Q of AlO_4 increases with the shear strain parameter, $|\psi|$, of the AlO_4 tetrahedron, which is defined by the following equation (2) [40]:

$$|\psi| = \sum_i |tan(\theta_i - \theta_{ideal})| \tag{2}$$

where the sum runs over the six O–Al–O bond angles θ_i [41] and θ_{ideal} is the ideal O–Al–O bond angle (109.5°), as illustrated in Figure 9. The derived C_Q values of the NAS and LAS glasses indicated that the shear strain was larger in the LAS system. High-temperature in-situ ^{29}Si NMR studies of alkali silicate melts [42] suggested that the breaking and reforming of Si–O bonds controlled the viscous flow. Similarly, it has been reported that the breaking and

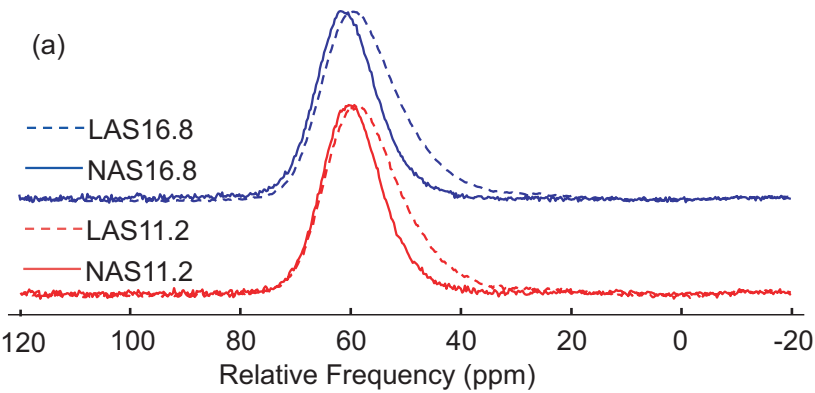

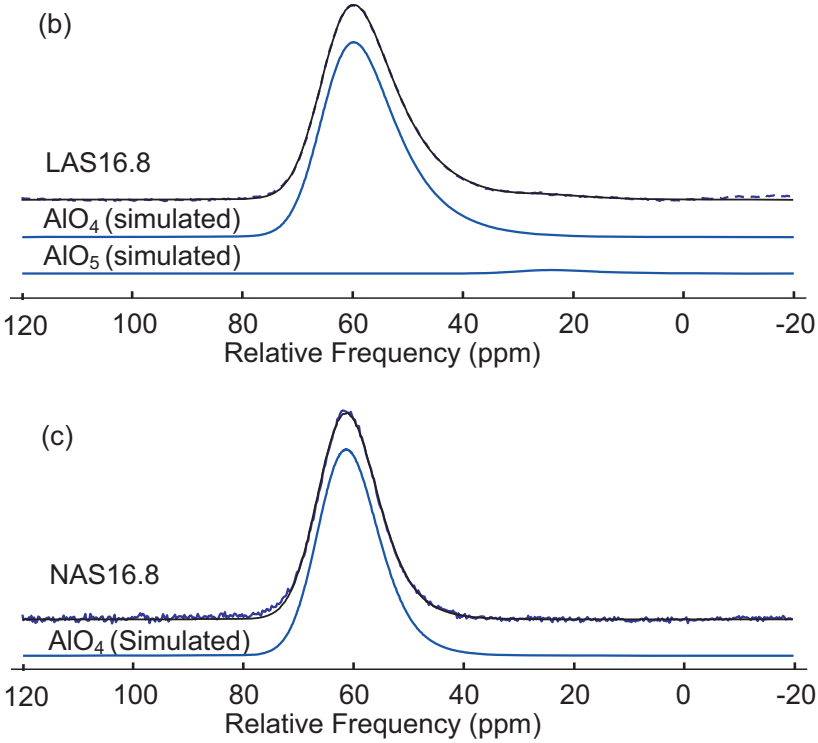

FIGURE 8
(a) ^{27}Al MAS NMR spectra of the NAS and LAS glasses. Fitting results for the ^{27}Al MAS NMR spectra of (b) LAS16.8 and (c) NAS16.8 glasses, as examples.

TABLE 3
Fitting parameters for ^{27}Al MAS NMR spectra of the glasses.

	AlO_4			AlO_5		
Sample	**Area (%)**	**δ_{iso}/ppm**	**C_Q/MHz**	**Area (%)**	**δ_{iso}/ppm**	**C_Q/MHz**
NAS11.2	100	64.2	4.0	-	-	-
NAS16.8	100	65.0	4.0	-	-	-
LAS11.2	98.3	64.2	5.1	1.7	28.4	5.1*
LAS16.8	98.2	65.1	5.2	1.8	29.3	5.2*

*Fixed parameter

reformation of T–O (T: Si or Al) is a rate-controlling step in the viscous flow of aluminosilicate melts [43]. Behrens and Schultz [44] proposed that the distortion of the O–T–O bond reduces the energy required to break the T–O bond. The observed C_Q of AlO_4 in the alkali aluminosilicate glasses indicated

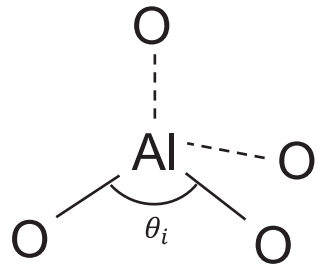

FIGURE 9
Schematic of local structure around an AlO_4 tetrahedron.

that the breaking and reformation of Al–O bonds in the lithium-containing system should be more pronounced than those in the sodium-containing system. Thus, the viscosity increased with an increase in the $AlO_{1.5}/SiO_2$ ratio and was greater for the NAS system than for the LAS system.

4 CONCLUSIONS

The $AlO_{1.5}/SiO_2$ molar ratio-induced changes in the viscosity of the alkali silicate systems were investigated using the rotating crucible method and DTA. The viscosity of the sodium silicate system drastically increased with increasing the ratio, whereas that of the lithium-containing system was not sensitive to this ratio. These results indicated that lithium-containing systems had the advantage of suppressing the viscosity increase due to the reaction between silicate melts and aluminum-containing steel in their continuous casting process. Moreover, structural characterization using Raman and ^{27}Al MAS NMR spectroscopy indicated that the aluminum cations in the selected silicate melts acted as network formers; however, the shear strain of the AlO_4 tetrahedron depended on the type of alkali cation present in the system. These results indicate that the degree of shear strain of the AlO_4 tetrahedron plays an important role in controlling the viscosity of aluminosilicate systems.

ACKNOWLEDGMENTS

This work was financially supported by JSPS KAKENHI (Grant Numbers 21H01854 and 16H04543) and the Research Program of “Dynamic Alliance for Open Innovation Bridging Human, Environment and Materials” in “Network Joint Research Center for Materials and Devices”.

REFERENCES

[1] Bezuidenhout, G.A., Pistorius, P.C. *Ironmak. Steelmak*, **27** (2000), 387, https://doi.org/10.1179/030192300677705

[2] Kim, M.-S., Lee, S.-W., Cho, J.-W., Park, M.-S., Lee, H.-G., Kang, Y.-B. *Metall. Mater. Trans. B,* **44** (2013), 299, https://doi.org/10.1007/s11663-012-9770-z

[3] Mills, K.C., Däcker, C.-Å. *Selection of mould fluxes and special mould fluxes for continuous casting*, in: *The casting powders book*; Cham: Springer; 2017, p. 393, https://doi.org/10.1007/978-3-319-53616-3_10

[4] Mills, K.C., Yuan, L., Li, Z., Zhang, G. *High Temp. High Press.*, **42** (2013), 237

[5] Deng, Y., Dan, Z., Yan, D., Wang, Q., He, S. *J. Mater. Res., Technol.*, **9** (2020), 9568, https://doi.org/10.1016/j.jmrt.2020.06.082

[6] Yan, X., Pan, W., Wang, X., Zhang, X., He, S., Wang, Q. *Metall. Mater. Trans. B*, **52** (2021), 2526, https://doi.org/10.1007/s11663-021-02200-y

[7] Lei, J., Yang, W., Sheng, G-Y., Zhang, C., Wu, T., Wang, H-C. *Metall. Mater. Trans. B*, **53** (2022), 2239, https://doi.org/10.1007/s11663-022-02523-4

[8] Zhang, Z., Wen, G., Tang, P., Sridhar, S. *ISIJ Int.*, **48** (2008), 739, https://doi.org/10.2355/isijinternational.48.739

[9] Liao, J., Zhang, Y., Sridhar, S., Wang, X., Zhang, Z. *ISIJ Int.*, **52** (2012), 753, https://doi.org/10.2355/isijinternational.52.753

[10] Zhang, G.-H., Chou, K.-C. *ISIJ Int.*, **53** (2013), 177, https://doi.org/10.2355/isijinternational.53.177

[11] Wang, Z., Sohn, I. *ISIJ Int.*, **60** (2020), 2705, https://doi.org/10.2355/isijinternational.ISIJINT-2019-522

[12] Wang, Z., Sohn, I. *Ceram. Int*., **46** (2020), 903, https://doi.org/10.1016/j.ceramint.2019.09.048

[13] Haghdani, S., Tangstad, M., Kristian Etienne, E. *Metall. Mater. Trans. B*, **53** (2022), 1733, https://doi.org/10.1007/s11663-022-02483-9

[14] Stebbins, J.F., Wu, J., Thompson, L.M. *Chem. Geol*., **346** (2013), 34, https://doi.org/10.1016/j.chemgeo.2012.09.021

[15] Neuville, D.R., Cormier, L., Massiot, D. *Chem. Geol.*, **229** (2006), 173, https://doi.org/10.1016/j.chemgeo.2006.01.019

[16] Sukenaga S., Shibata H. *High-temperature characterization of glasses and melts*, in: *Encyclopedia of Materials: Technical Ceramics and Glasses*; M. Pomeroy (Ed.); Oxford: Elsevier; 2021, p. 689.

[17] Sukenaga, S., Ogawa, M., Yanaba, Y., Ando, M., Shibata, H. *ISIJ Int.*, **60** (2020), 2794, https://doi.org/10.2355/isijinternational.ISIJINT-2020-326

[18] Sukenaga, S., Ogawa, M., Yanaba, Y., Ando, M., Shibata, H. *Tetsu-to-Hagane*, **108** (2022), 175, https://doi.org/10.2355/tetsutohagane.TETSU-2021-108

[19] Kim K.-H., Sukenaga S., Tashiro M., Kanehashi K., Yoshida S., Shibata H. *J. Non-Cryst. Solids*, **587** (2022), 121600, https://doi.org/10.1016/j.jnoncrysol.2022.121600

[20] Sukenaga, S., Nagahisa, T., Kanehashi, K., Saito, N., Nakashima, K. *ISIJ Int.*, **51** (2011), 333, https://doi.org/10.2355/isijinternational.51.333

[21] Sukenaga, S., Unozawa, H., Chiba, Y., Tashiro, M., Kawanishi, S., Shibata, H. *J. Am. Ceram. Soc.*, **106** (2023), 293, https://doi.org/10.1111/jace.18760

[22] Babcock, C.L. *J. Am. Ceram. Soc.*, **17** (1934), 329, https://doi.org/10.1111/j.1151-2916.1934.tb19333.x

[23] Neuville, D.R. *Chem. Geol.*, **229** (2006), 28, https://doi.org/10.1016/j.chemgeo.2006.01.008

[24] Lillie, H.R. *J. Am. Ceram. Soc.*, **22** (1939), 367, https://doi.org/10.1111/j.1151-2916.1939.tb19482.x

[25] Preston, E. *J. Soc. Glass Technol*., **22** (1938), 45

[26] Bockris, J.O.M., Mackenzie, J.D., Kitchener, J.A. *Trans. Faraday Soc.*, **51** (1955), 1734, https://doi.org/10.1039/TF9555101734

[27] Shartsis, L., Spinner, S., Capps, W. *J. Am. Ceram. Soc.*, **35** (1952), 155, https://doi.org/10.1111/j.1151-2916.1952.tb13090.x

[28] Al-Mukadam, R., Di Genova, D., Bornhöft, H., Deubener, J. *J. Non-Cryst. Solids*, **536** (2020), 119992, https://doi.org/10.1016/j.jnoncrysol.2020.119992

[29] Koontz E. *Thermal analysis of glass*, in: *Springer handbook of glass*, Musgraves, J.D., Hu, J., Calvez, L. eds.; Cham: Springer; 2019, p. 853-878, https://doi.org/10.1007/978-3-319-93728-1_24
[30] Nascimento, M.L.F., Fokin, V.M., Zanotto, E.D., Abyzov, A.S. *J. Chem. Phys.*, **135** (2011), 194703, https://doi.org/10.1063/1.3656696
[31] Le Losq, C., Neuville, D.R., Florian, P., Henderson, G.S., Massiot, D. *Geochim. Cosmochim. Acta*, **126** (2014), 495, https://doi.org/10.1016/j.gca.2013.11.010
[32] Neuville, D.R., De Ligny, D., Henderson, G.S., *Rev. Mineral. Geochem.*, **78** (2014), 509, https://doi.org/10.2138/rmg.2013.78.13
[33] Galeener, F.L. *Solid State Comm.*, **44** (1982), 1037, https://doi.org/10.1016/0038-1098(82)90329-5
[34] Mysen, B.O., Lucier, A., Cody, G.D. *Am. Mineral.*, **88** (2003), 1668, https://doi.org/10.2138/am-2003-11-1206
[35] Furukawa, T., Fox, K.E., White, W.B. *J. Chem. Phys.*, **75** (1981), 3226, https://doi.org/10.1063/1.442472
[36] Sukenaga, S., Florian, P., Kanehashi, K., Shibata, H., Saito, N., Nakashima, K., Massiot, D. *J. Phys. Chem. Lett.*, **8** (2017), 2274, https://doi.org/10.1021/acs.jpclett.7b00465
[37] Allwardt, J.R., Lee, S.K., Stebbins, J.F. *Am. Mineral.*, **88** (2003), 949, https://doi.org/10.2138/am-2003-0701
[38] Lee S.K., Stebbins J.F. *J. Phys. Chem. B*, **104** (2000) 4091, 10.1021/jp994273w
[39] Massiot, D., Fayon, F., Capron, M., King, I., Le Calvé, S., Alonso, B., Durand, J.-O., Bujoli, B., Gan, Z., Hoatson, G. *Magn. Reson. Chem.*, **40** (2002), 70, https://doi.org/10.1002/mrc.984
[40] MacKenzie, K.J.D., Smith, M.E.; *^{27}Al NMR* in: *Pergamon Materials Series, Pergamon*; Elsevier: Amsterdam; 2002, p. 271, https://doi.org/10.1016/S1470-1804(02)80006-2
[41] Engelhardt, G., Koller, H., Sieger, P., Depmeier, W., Samoson, A. *Solid State Nucl. Magn. Reson*., **1** (1992), 127, https://doi.org/10.1016/0926-2040(92)90013-Y
[42] Farnan, I., Stebbins, J.F. *J. Am. Chem. Soc.*, **112** (1990), 32, https://doi.org/10.1021/ja00157a008
[43] Gruener, G., Odier, P., De Souza Meneses, D., Florian, P., Richet, P. *Phys. Rev. B.*, **64** (2001), 024206, https://doi.org/10.1103/PhysRevB.64.024206
[44] Behrens, H., Schulze, F. *Am. Mineral.*, **88** (2003), 1351, https://doi.org/10.2138/am-2003-8-919